



## Non-linear system identification using closed-loop data with no external excitation: the case of a lean combustion chamber

SERGIO M. SAVARESI†\*, ROBERT R. BITMEAD‡ and WAYNE J. DUNSTAN‡

This paper deals with the analysis of a set of measurements collected on a lean premixed combustion process operating in a limit cycle. Due to the fact that the data are collected in closed-loop and the system has no external excitation, the identification task is particularly challenging. This work mainly focuses on the issue of the feasibility of the identification task. It will be shown that, despite the paucity of information available, a grey-box non-linear model can be estimated. The model provides an explanation both of the limit-cycle fundamental oscillation and of a non-harmonic high-frequency signal affecting the pressure of the combustion chamber.

### 1. Introduction

The aim of this paper is to discuss the problem of analysing, interpreting, and modelling a set of data collected on a real process. The specific process is a lean premixed combustion process, as one might find in a gas turbine or jet engine, where the dynamics appear to be governed by self-excited oscillations, whose frequency, phase and amplitude depend on the current fuel-to-air ratio.

The measured signals are the pressure and the heat release rate at the burning plane recorded from the UTRC/DARPA (United Technologies Research Corporation/Defense Advanced Research Projects Agency) single nozzle rig experiment. This is part of an experimental programme conducted by UTRC, with the objective of demonstrating the applications of active control to lean premixed combustion systems.

The system is limit cycling. Because the measurements are collected in closed-loop, the system has no external excitation, the data are effectively purely periodic and are filtered by the measurement device, the identification of a model of the process is very challenging. The first question to be addressed is, therefore, the system identifiably given the data.

Some interesting results can be obtained thanks to *a priori* information embedded in a parametrized 'grey-box' physical model. Specifically, the model provides an explanation both of the limit-cycle fundamental oscillation and of a non-harmonic high-frequency signal affecting the pressure of the combustion chamber. On the basis of this model structure it is possible to comment on the experiment, and to interpret the data. This work is an example of non-linear dynamic system iden-

tification with the uncertainties of real world modelling from experimental data.

The problem of modelling and understanding the phenomenon of combustion instability in lean premixed combustors has received a great deal of interest in recent years, due to the significant advantages, mainly in pollution control and fuel consumption, inherently yielded by lean combustion. Refer to Culick (1976), Annaswamy and Ghoniem (1995), Isella *et al.* (1997) and Baldini *et al.* (1999) for examples. The main contribution of this paper, and its most peculiar feature, is to focus on the problem of extracting the maximum amount of information from a few sets of measured data in limit cycle, in order to validate or invalidate a given model. We emphasize the tight relationship between a model and the available data, showing that non-linear identification is a genuine two-way process: not only can a physical model help to interpret and fit a set of data, but data analysis can help to modify suitably, or understand better, a physical model.

The starting point of this work is from Peracchio and Proscia (1998), where the local model is derived from physical principles. This model structure provides the basis for a significant data analysis in Murray *et al.* (1998), which we amplify and extend. Using the same sets of data, the aim of the present paper is to make a step further, in order to give a comprehensive and homogeneous interpretation of all the features of the data set.

The outline of the paper is as follows. In §2 the measured data are briefly discussed and analysed, and the relationship, in terms of phase and magnitude, between the two measured signals at the fundamental frequency is estimated. Section 3 is devoted to the problem of estimating the parameters of a physical model of the fundamental limit-cycling oscillation. In §4 the spectral content of the signals beyond the fundamental frequency is considered. In particular, the problem of modelling a non-harmonic oscillation at 750 Hz is addressed. Some cautionary remarks form the conclusion.

---

Received for publication 16 August 2001.

\* Author for correspondence.

† Dipartimento di Elettrotecnica e Informazione, Politecnico di Milano, Piazza L. da Vinci, 32, 20133, Milan, Italy.

‡ Department of Mechanical and Aerospace Engineering, University of California San Diego, 9500 Gilman Drive, La Jolla, CA 92039-0411, USA.

## 2. The measured data: a preliminary analysis

The only signals measured and recorded on the UTRC/DARPA single nozzle ring experiment are the pressure  $p$  and the heat release rate  $q$ . Both  $p$  and  $q$  are measured in the combustion chamber at the burning plane, whose longitudinal position is supposedly almost constant. During the set of experiments, collectively labelled R228, six pairs of  $p$ - $q$  measurements were collected, corresponding to six different values of equivalence ratio  $\phi$  (table 1). The equivalence ratio is a crucial parameter in the context of lean combustion; it is defined as

$$\phi = \frac{(W_F/W_A)}{(W_F/W_A)_S}$$

where  $W_F$  and  $W_A$  are the fuel and air mass flows injected at the nozzle per unit of time. The subscript ‘S’ denotes the stoichiometric value of the fuel-to-air ratio. A standard stoichiometric combustion is characterized by  $\phi = 1$ . Note that the UTRC/DARPA trials have been performed at much lower equivalence ratios, in order to test fully and understand the limits of a lean combustion process.

In the sequel, the sets of data collected during the six trials will be analysed under the assumption that they are cyclo-stationary signals. It is important to stress that this assumption is well satisfied by the signals of Experiments 1–4. It is not fully true for the signals of Experiments 5 and 6, which are quite irregular and show some time-dependent features. This is due to the fact that the combustion process that takes place at a very low equivalence ratio is on the limit of stability: it has a very irregular behaviour, and tends to fade away. Therefore, the results concerning these two sets of data are not as reliable as those concerning the Data Sets 1 to 4.

In figure 1, the  $p$  and  $q$  signals of Experiment 1 are displayed over an 80 ms time window, while in figure 2 their power spectra are displayed over the 0–1000 Hz range. The signals measured in the other experiments show similar behaviour. From a preliminary analysis of the data in figure 1 and in figure 2, the following can be said:

- $q$  and  $p$  are characterized by a main non-damped oscillation at about 210 Hz; since there is no external persistent excitation, the system must be affected by a limit-cycle phenomenon. Notice that this is possibly only if the system is character-

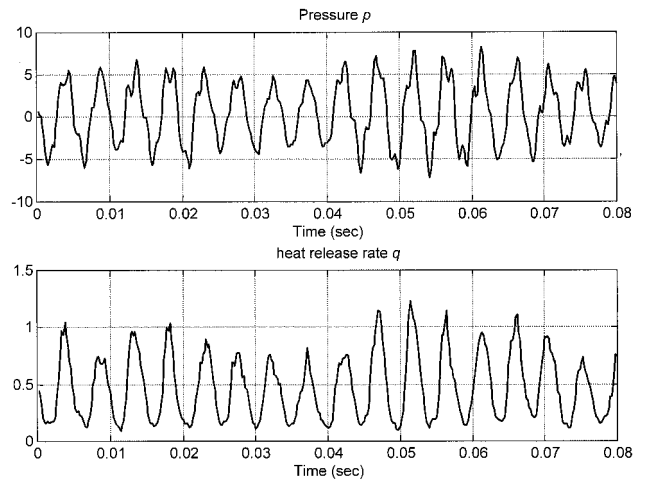


Figure 1. Signals registered in Experiment 1 (80 ms time-window).

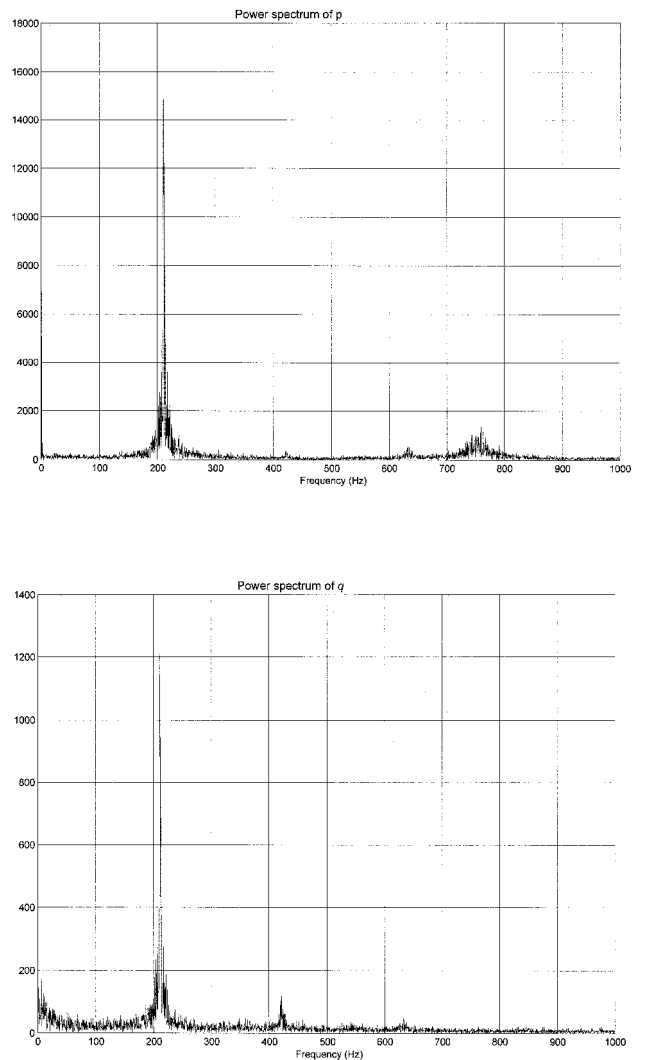


Figure 2. (a) Power spectrum of  $p$  (Experiment 1). (b) Power spectrum of  $q$  (Experiment 1), with DC component removed.

Experiment number	1	2	3	4	5	6
Equivalence ratio $\phi$	0.56	0.53	0.51	0.49	0.47	0.45

Table 1. UTRC/DARPA experiments (sampling frequency 5000 Hz; 16 000 samples available for each experiment).

Experiment	Equivalence ratio $\phi$	Frequency $\tilde{\omega}$ of the limit-cycle	Phase-shift from $q$ to $p$ , at the limit-cycle frequency $\tilde{\omega}$	Gain from $q$ to $p$ , at the limit-cycle frequency $\tilde{\omega}$
1	0.56	219.9 Hz	$-5.74^\circ$	12.14
2	0.53	209.1 Hz	$-9.44^\circ$	13.15
3	0.51	205.7 Hz	$-14.35^\circ$	14.79
4	0.49	202.7 Hz	$-19.18^\circ$	16.05
5	0.47	198.4 Hz	$-22.92^\circ$	18.80
6	0.45	179.8 Hz	$-42.72^\circ$	45.01

Table 2. Estimated characteristics of the self-excited limit-cycle oscillations.

ized by a non-linear element (e.g. a saturation effect).

- Both  $p$  and  $q$  are mainly constituted by periodic signals; the broad-band content of  $p$  and  $q$  is negligible.
- The periodic signals constituting  $q$  and/or  $p$  are three harmonically-related signals, at about 210 Hz, 420 Hz and 640 Hz, and a non-harmonic signal, as about 750 Hz.
- Only three sinusoidal signals are really detectable in  $p$  and  $q$ : the first harmonic signal in  $p$  and in  $q$ , and the non-harmonic signal in  $p$ . The second and third harmonic signals in  $p$  and  $q$  are extremely small, whereas the non-harmonic signal is totally absent in  $q$ .

According to the above remarks, the most important and reliable piece of information is the relationship in phase and magnitude of the fundamental oscillation in  $p$  and  $q$ . This piece of information will be used extensively throughout the paper.

The estimation of the relationship in terms of phase and amplitude of the fundamental oscillation in  $p$  and  $q$  can be obtained using many techniques (see, e.g. Bitmead *et al.* 1986, Young 1999, and references cited therein). Among them, the Fast-Fourier-Transform (FFT) is a widely known technique for spectral analysis. Using 16 000 data snapshots of a signal sampled at 5000 Hz, one can obtain an estimate of the spectral content of the signal, with a resolution of approximately  $5000/16\,000 = 0.31$  Hz.

The estimate of the limit-cycle frequency  $\tilde{\omega}$  can be obtained as the frequency where  $\text{FFT}[p(t)]$  has a maximum. The estimate of the phase shift and gain from  $q$  to  $p$  at  $\tilde{\omega}$  can be obtained as  $\angle\{\text{FFT}[p(t)]/\text{FFT}[q(t)]\}$  and  $|\text{FFT}[p(t)]/\text{FFT}[q(t)]|$ , respectively, evaluated at  $\tilde{\omega}$ . In order to reduce the variance of the estimated phase-shift and gain we used a weighted average of the estimated phase-shifts and gains, over 11 values around  $\tilde{\omega}$  (the weights are the amplitude of the harmonic component). The estimation results are listed in Table 2.

### 3. Modelling the fundamental oscillation

Due to the periodicity of the signals and the corresponding paucity of information available from the measured data, the estimation of a non-linear dynamic model of the combustion process in a black-box fashion (e.g. using approximation tools like Volterra series or neural networks) is barely feasible. Some *a priori* knowledge of the system must be taken into account. The most intuitive and natural way of using *a priori* knowledge is to resort to physical modelling of the process. The knowledge of the main phenomena occurring during combustion yields the main structure of the model; its parameters then can be estimated on the basis of the measured data. This mixed use of physical modelling and data based identification is usually called ‘grey-box modelling’.

In this section we will focus on the first harmonic oscillation only; it is the main part of the measured signals. The analysis and modelling of the remaining parts of signals  $p$  and  $q$  will be considered in the next section.

The first-principles model used here to fit the measured signals  $p$  and  $q$  has been mainly developed in Peracchio and Proscia (1998). It has the structure displayed in figure 3, where:

- $p$  is the pressure at the burning plane;

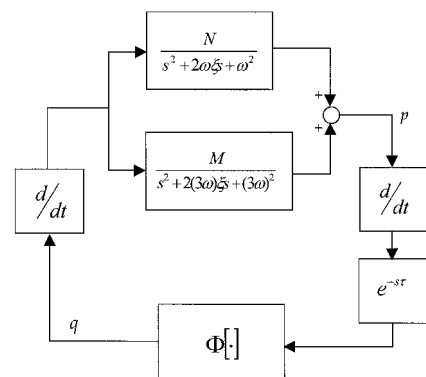


Figure 3. Block diagram of the first-principles model.

- $\Phi[\cdot]$  is a static non-linear mapping; physical considerations suggest that this mapping should be characterized by a non-positive slope;
- $q = \Phi[\dot{p}(t - \tau)]$  is the heat release rate at the burning plane;
- $\omega$ ,  $\xi$  and  $N$  are the central frequency, damping, and scaling factors of the second-order oscillator representing the first (main) acoustic resonance of the combustor;  $M$  is the scaling factor of the third acoustic resonance.
- $\tau$  is a time delay; specifically, it is the time taken by the mixed gas at the nozzle to reach the burning plane at the end of the combustion chamber.

This model is derived by the Navier–Stokes equations, which provide the density, pressure and velocity fields in the combustion chamber, and by an energy-balance equation. Note that the model does not contain partial derivatives: it is obtained by expanding the solution of the distributed-parameter model into the orthogonal acoustic modes of the systems, defined by an eigenvalue problem, and picking up the first and third modes.

This model is a simple mathematical description of the following physical phenomena (see figure 3, clockwise):

- the pressure  $p$  is characterized by acoustic resonant modes; as usual, they are modelled with slightly damped second-order oscillators. First and third harmonic oscillators allow a good explanation of the data (see §4), while keeping the model complexity comparatively low. Physically, they describe a semi-open or ‘organ-pipe’ acoustical model of the combustion chamber;
- the normalized flow speed is proportional to the time derivative of the pressure;
- the heat release rate  $q$  is proportional to the delayed flow speed, distorted by a non-linear characteristic  $\Phi[\cdot]$ ; the delay is the travelling time taken by the mixed gas to reach the burning plane from the nozzle.
- the time derivative of the heat release is the input of the second-order oscillator.

The model in figure 3 summarizes the *a priori* knowledge of the physical phenomena taking place during the combustion process. It can be complemented with another piece of *a priori* information: the occurrence of a limit cycle. This is the only way of explaining the fact that  $p$  and  $q$  are characterized by a persistent oscillation, despite the system having no external excitation. Notice that the limit-cycling behaviour is compatible with the model, because of the non-linear static characteristic  $\Phi[\cdot]$ . The *a priori* information on the occurrence

of a limit-cycle behaviour can be formally expressed by the following two conditions (Gelb and Van der Velde 1968):

- The phase shift of the linear part of the loop must be exactly equal to  $180^\circ$  (we assume that the slope of  $\Phi[\cdot]$  at zero is negative), at the observed limit-cycle frequency  $\tilde{\omega}$

$$\mathcal{L} \left\{ \left( \frac{Ns^2 e^{\tau s}}{s^2 + 2\omega\xi s + \omega^2} + \frac{Ms^2 e^{-\tau s}}{s^2 + 2(3\omega)\xi s + (3\omega)^2} \right) \right\}_{s=j\tilde{\omega}} = 180^\circ \quad (1a)$$

- The loop must be ‘unstable’ at  $\tilde{\omega}$ , namely the local gain of the loop at  $\tilde{\omega}$  must be larger than 1

$$\left| \left( \frac{Ns^2 e^{-\tau s}}{s^2 + 2\omega\xi s + \omega^2} + \frac{Ms^2 e^{-\tau s}}{s^2 + 2(3\omega)\xi s + (3\omega)^2} \right) \Phi'(0) \right\}_{s=j\tilde{\omega}} > 1 \quad (1b)$$

where  $\Phi'(0)$  is the slope of the non-linear characteristic about zero.

The physical model and condition (1) strongly reduce the complexity of the problem of estimating a non-linear dynamic model of the combustion process. In particular, notice that since condition (1a) is an ‘equality’ constraint, it can be effectively exploited for parameter estimation.

The grey-box identification problem reduces to the data-based estimation of parameters  $\{\omega, \xi, N, M, \tau\}$  and function  $\Phi[\cdot]$ . This issue will be treated in the rest of this section. In §3.1, the problem of estimating  $\tau$  will be addressed; §3.2 will be devoted to the estimation of  $\Phi[\cdot]$ , whereas in §3.3 the identification of the parameters  $\{\omega, \xi, N, M\}$  of the second-order oscillators will be discussed.

### 3.1. Estimation of the time-delay $\tau$

The time delay  $\tau$  can be estimated as the phase shift between  $q$  and  $p$  at the limit-cycle frequency. Condition (1a) can be rewritten as

$$\mathcal{L} \left\{ \left( \frac{Ns}{s^2 + 2\omega\xi s + \omega^2} + \frac{Ms}{s^2 + 2(3\omega)\xi s + (3\omega)^2} \right) \right\}_{s=j\tilde{\omega}} + \mathcal{L}\{s\}_{s=j\tilde{\omega}} + \mathcal{L}\{e^{-\tau s}\}_{s=j\tilde{\omega}} = 180^\circ \quad (2)$$

namely  $\hat{\Delta}(\tilde{\omega}) + 90^\circ - \tau\tilde{\omega} \cdot 360^\circ = 180^\circ$ , where  $\tilde{\omega}$  is the limit-cycle frequency measured in Hz, and  $\hat{\Delta}(\tilde{\omega})$  is the phase-shift from  $q$  to  $p$  at  $\tilde{\omega}$ , measured in degrees. Since (see table 2)  $\hat{\Delta}(\tilde{\omega})$  always takes negative values, and  $\tau$  must be positive, in the above expression  $\hat{\Delta}(\tilde{\omega})$  must be replaced by  $360^\circ + \hat{\Delta}(\tilde{\omega})$ , so obtaining

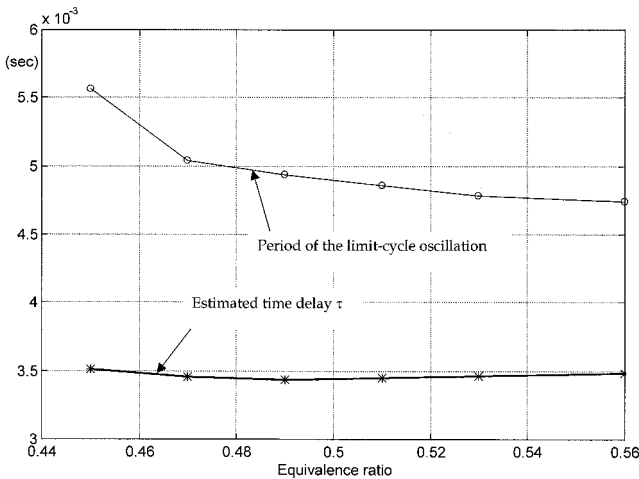


Figure 4. Estimated delay (compared to the period of the limit-cycle oscillation).

$$\tau = \frac{(360^\circ + \hat{\Delta}(\tilde{\omega}) - 90^\circ)}{\tilde{\omega} \cdot 360^\circ} \quad (3)$$

Substituting the results displayed in table 2 into (3) gives an estimate of the time delay. The results are displayed in figure 4. It is interesting to note that the time taken by the mixed gas at the nozzle to reach the burning plane is almost constant, namely it is not a function of the equivalence ratio  $\phi$ .

### 3.2. Estimation of the non-linear characteristic $\Phi[\cdot]$

The estimation of the static non-linear characteristic  $\Phi[\cdot]$  is, in principle, a simple task, once the time delay  $\tau$  is estimated. It can be obtained by plotting  $q(t)$  vs.  $\dot{p}(t - \tau)$ . Obviously, because of noise, unmodelled phenomena, and disturbances, a scattered  $q(t) \leftrightarrow \dot{p}(t - \tau)$  plot is expected. The best results in terms of minimization of the scattering of the  $q(t) \leftrightarrow \dot{p}(t - \tau)$  plot are obtained by approximating  $\dot{p}(t)$  as

$$\dot{p}(t) = \tilde{\omega} p \left( t + \frac{1}{4} \frac{2\pi}{\tilde{\omega}} \right) \quad (4)$$

where  $\tilde{\omega}$  is the estimated limit-cycle frequency measured in Hz. This result, found empirically, has a simple interpretation. Approximation (4) corresponds to a  $+90^\circ$  phase shift of a sinusoidal signal at frequency  $\tilde{\omega}$ . Replacing the first derivative of  $p(t)$  with (4) hence corresponds to considering  $q(t)$  and  $p(t)$  as constituted by the fundamental oscillation only. This is preferable since higher order harmonics in  $q(t)$  and  $p(t)$  are either small or asymmetric (namely  $q(t)$  lacks some sinusoidal components which are in  $p(t)$ ). In figure 5, the plot of  $q(t)$  vs.  $\dot{p}(t - \tau)$  is displaced (Experiment 2).

In order to get an estimate of the nonlinear characteristic, a scatter-plot smoothing technique must be used. Here we use the simple method of dividing the points into narrow vertical bins, and averaging the

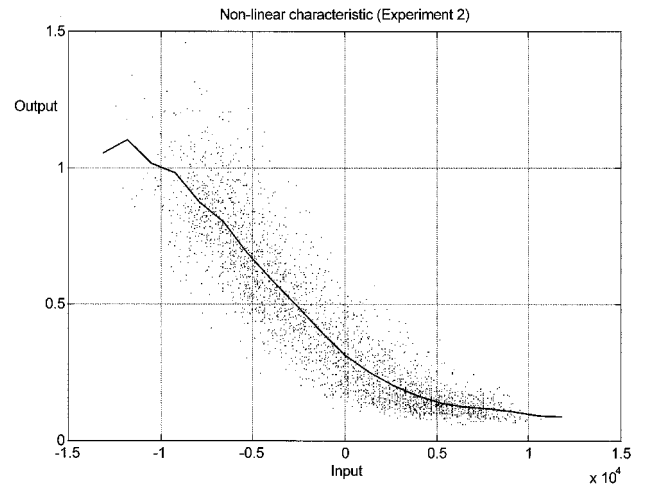


Figure 5. Scatter plot of  $q(t)$  vs.  $\dot{p}(t - \tau)$ , and the corresponding estimated characteristic (Experiment 2).

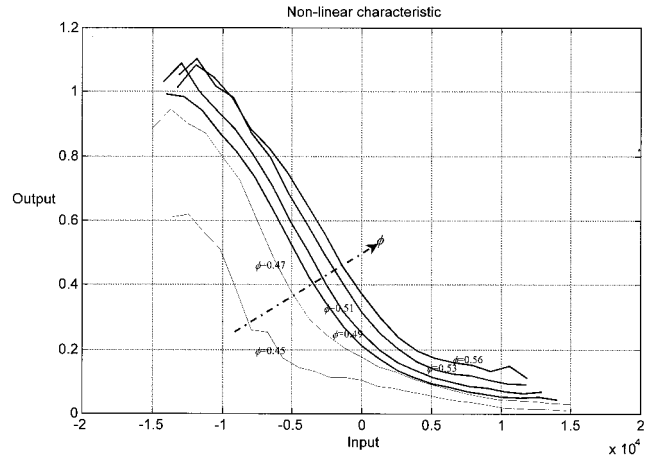


Figure 6. Estimated non-linear characteristics from scatter plots of  $q(t)$  vs.  $\dot{p}(t - \tau)$ , for different values of  $\phi$ .

value of the outputs within the bin. This method is quite crude, but it is adequate for the purpose of this analysis. The results of this averaging procedure are summarized in figure 6. It can be noticed that, as  $\phi$  decreases,  $\Phi[\cdot]$  slightly drifts to the left and becomes flatter.

From the estimated non-linear characteristics it is possible to compute  $\Phi'[\cdot]$ , the first derivative of the characteristic about zero. Such a parameter plays a crucial role (see (1 b)) in determining the stability of the overall loop and, therefore, the existence of a limit-cycle. The estimated values of  $\Phi'[\cdot]$  are summarized in Table 3. Notice that the absolute value of the gain becomes smaller as the equivalence ratio decreases. It is important to stress that, as  $\phi$  decreases, the plot of  $q(t)$  vs.  $\dot{p}(t - \tau)$  is more and more scattered. The estimation of  $\Phi'[0]$  for low values of  $\phi$  hence is expected to be less accurate.

Experiment number	1	2	3	4	5	6
Equivalence ratio $\phi$	0.56	0.53	0.51	0.49	0.47	0.45
$\Phi'[0]$ (local gain at zero)	$-0.703 \times 10^{-4}$	$-0.707 \times 10^{-4}$	$-0.670 \times 10^{-4}$	$-0.626 \times 10^{-4}$	$-0.401 \times 10^{-4}$	$-0.0872 \times 10^{-4}$

Table 3. Estimated gains of the non-linear characteristic about zero.

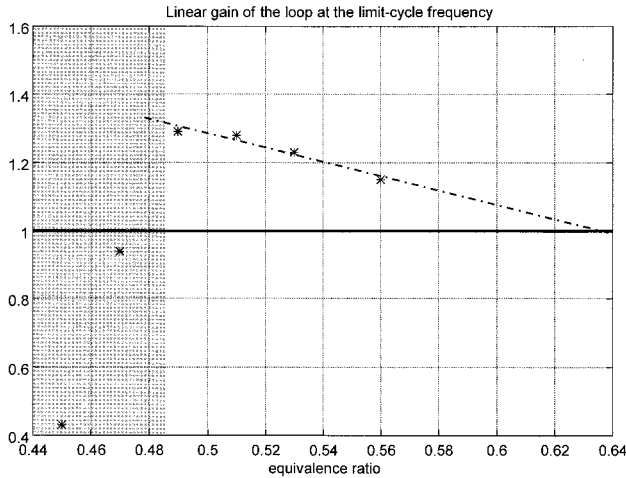


Figure 7. Estimated gains of the loop (indicated with the symbol ‘\*’).

We conclude this subsection by checking the constraint (1 b), which must be fulfilled in order to yield a limit-cycle. To this end, the loop gains at the limit-cycle frequency are displayed in figure 7. They are computed using the gains from  $q$  to  $p$  (table 2), and the values of  $\Phi'[0]$  (table 3). By inspecting such results, we can say that:

- The constraint is fulfilled for the first four experiments; it is not fulfilled for very low values of equivalence ratio ( $\phi = 0.47$ , and  $\phi = 0.45$ ). In such cases, however, the non-fulfillment of the constraint is due to poor estimation of the local gain of the non-linear function, which is subject to high uncertainties, largely because of the failure of the periodicity assumption.
- The local gain of the loop decreases regularly in a linear fashion as the equivalence ratio increases. Moreover, such a gain is only slightly higher than 1. As a consequence, by inspecting figure 7 it can be roughly predicted that the limit-cycle phenomenon should vanish for values of  $\phi$  higher than about 0.64.

### 3.3. Estimation of the second-order oscillator

The last part of the model to be estimated is the path from  $q$  to  $p$ , namely

$$G(s) = \frac{Ns}{s^2 + 2\omega\xi s + \omega^2} + \frac{Ms}{s^2 + 2(3\omega)\xi s + (3\omega)^2}$$

$G(s)$  is characterized by four parameters  $\{M, N, \xi, \omega\}$ , which, in principle, are all functions of  $\phi$ . Using the estimated  $q$ - $p$  phase-shift  $\hat{\Delta}(\tilde{\omega})$  and gain  $\hat{A}_p(\tilde{\omega})/\hat{A}_q(\tilde{\omega})$  of  $G(s)$  at the limit-cycle frequency  $\tilde{\omega}$ , for each value of  $\phi$  the following two relationships can be written

$$\left. \begin{aligned} \left| \frac{Ns}{s^2 + 2\omega\xi s + \omega^2} + \frac{Ms}{s^2 + 2(3\omega)\xi s + (3\omega)^2} \right|_{s=j\tilde{\omega}} &= \frac{\hat{A}_p(\tilde{\omega})}{\hat{A}_q(\tilde{\omega})} \\ \angle \left[ \frac{Ns}{s^2 + 2\omega\xi s + \omega^2} + \frac{Ms}{s^2 + 2(3\omega)\xi s + (3\omega)^2} \right]_{s=j\tilde{\omega}} &= \hat{\Delta}(\tilde{\omega}) \end{aligned} \right\} \quad (5a)$$

Note that at  $s = j\tilde{\omega}$  the term due to the third-harmonic oscillator can be neglected. Henceforth (5 a) becomes

$$\left. \begin{aligned} \left| \frac{Ns}{s^2 + 2\omega\xi s + \omega^2} \right|_{s=j\tilde{\omega}} &\approx \frac{\hat{A}_p(\tilde{\omega})}{\hat{A}_q(\tilde{\omega})} \\ \angle \left[ \frac{Ns}{s^2 + 2\omega\xi s + \omega^2} \right]_{s=j\tilde{\omega}} &\approx \hat{\Delta}(\tilde{\omega}) \end{aligned} \right\} \quad (5b)$$

which, after simple manipulations, can be rewritten as

$$\left. \begin{aligned} \frac{N\tilde{\omega}}{\sqrt{(\omega^2 - \tilde{\omega}^2)^2 + 4\xi^2\omega^2\tilde{\omega}^2}} &\approx \frac{\hat{A}_p(\tilde{\omega})}{\hat{A}_q(\tilde{\omega})} \\ 90^\circ - \arctan \left[ \frac{2\xi\omega\tilde{\omega}}{\omega^2 - \tilde{\omega}^2} \right] &\approx \hat{\Delta}(\tilde{\omega}) \end{aligned} \right\} \quad (5c)$$

Apparently, parameters  $\{M, N, \xi, \omega\}$  cannot be uniquely determined for each  $\phi$  since only two independent relationships are available. In particular,  $M$  is not identifiable via (5 c). This is intuitive since (5 c) uses information at  $\tilde{\omega}$  only (a frequency which is well away from the central frequency of the third-order harmonic oscillator). Henceforth, in the rest of this section, we shall restrict our attention to the first-harmonic oscillator only, namely

$$G(s) = \frac{Ns}{s^2 + 2\omega\xi s + \omega^2}$$

Some attempts (Murray 1998, Savaresi *et al.* 2000) have been made in order to try to extract additional information from the signal in the neighbourhood of the central

limit-cycling frequency  $\tilde{\omega}$ . The results obtained proved to be quite unsatisfactory due to the system being excited just over a very narrow bandwidth around the limit cycling frequency. We can therefore conclude that there exists an infinite set of models  $G(s, \phi)$ , which fulfil (5) and hence are compatible with or ‘unfalsified’ by the available data.

Despite this seemingly irresolvable indetermination, it is still interesting to discuss briefly the problem of restricting the class of unfalsified models, on the basis of additional qualitative reasoning.

First, from inspection of equations (5 c), the following remarks can be drawn:

- The second-order oscillator aims to model a persistent acoustic resonant mode. Hence, in order to yield a persistent resonance, the damping ratio  $\xi$  of the second-order oscillator must be small.
- Since the estimated phase shift  $\hat{\Delta}(\tilde{\omega})$  from  $q$  to  $p$  is comparatively small (except for the lowest value of  $\phi$ ), the second equation of (5 c) can be approximately rewritten as  $\arctan [2\xi\omega\tilde{\omega}/(\omega^2 - \tilde{\omega}^2)] \approx 90^\circ$ . If  $\xi$  is small, this means that  $\omega \approx \tilde{\omega}$ , namely the limit-cycling frequency is in the neighbourhood of the central frequency of the second-order oscillator.
- In order that the second equation of (5 c) be fulfilled,  $\tilde{\omega}$  must be always larger than  $\omega$ . This can be easily understood with the help of figure 8, where the Bode diagrams of  $G(s)$  for a specific choice of the parameters ( $N = 100$ ,  $\xi = 0.2$ ,  $\omega = 2\pi \cdot 200$ ) are plotted. Note that at  $\omega$  the phase shift induced by  $G(s)$  is exactly zero. Before  $\omega$  the phase shift is positive and beyond  $\omega$  the phase shift is negative.

Starting from the above remarks, physical considerations lead to the formulation of the following two

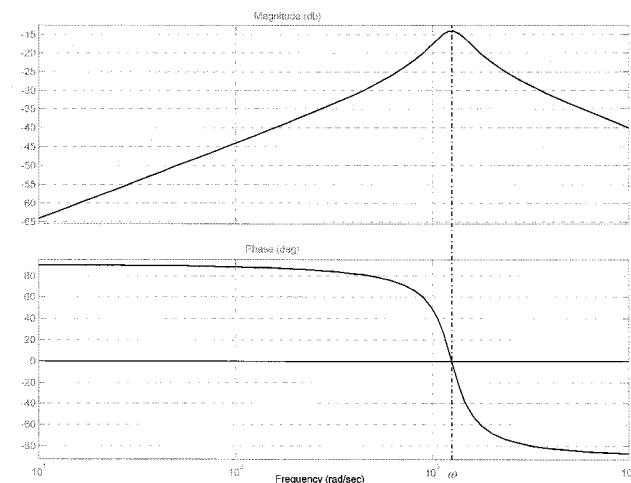


Figure 8. Bode diagrams of  $G(s)$  (first oscillator only) when  $N = 100$ ,  $\xi = 0.2$ ,  $\omega = 2\pi \cdot 200$ .

qualitative conditions, which can be added to the analytic conditions (5 c):

- It is reasonable to assume that the central frequency  $\omega$  of the second-order oscillator should not be subject to large variations, for different values of  $\phi$ . The central frequency  $\omega$  of the oscillator is the natural frequency of the first acoustic mode. As such, it is linked mainly to the geometrical features of the combustion chamber, which do not vary with  $\phi$ . Notice that this is true under the assumption that the position of the burning plane is fixed. Some recent studies (see e.g. Baldini *et al.* 1999) however, showed that this assumption is not rigorously true; this could explain small variations of  $\omega$  when  $\phi$  changes.
- It is reasonable to assume that the damping ratio  $\xi$  tends to increase with  $\phi$ . This is consistent with the fact that, as  $\phi$  grows, the limit-cycling oscillation tends to vanish, whereas for small values of  $\phi$  the limit-cycle phenomenon is so strong and undamped that it leads to an irregular combustion.

As an example, a set of six models compatible with the measured data, which also fulfil the above ‘qualitative’ conditions, is displayed in figure 9(a) (magnitude) and figure 9(b) (phase).

#### 4. Modelling the system beyond the fundamental oscillation

This section is devoted to the analysis, modelling and interpretation of the measured signals in the bandwidth beyond the frequency of the fundamental oscillation. As already said, this is a ‘marginal’ part of the signal in terms of spectral power; however, something interesting can be said about this part of the signal also.

By inspection of the spectral features of the measured signals  $p$  and  $q$  in figure 2(a) and (b) respectively, it is apparent that, in order to give an exhaustive and comprehensive interpretation of the data, the following two peculiar characteristics must be explained:

- The spectra of  $p$  and  $q$ , beyond the limit-cycle frequency, are incompatible with the model in figure 3. Pressure  $p$  is characterized by two clearly visible spectral components: a narrow-band signal at about 640 Hz (the frequency of the third harmonic) and a non-harmonic narrow-band signal at about 750 Hz. However, neither of these is in the power spectrum of  $q$ . This contradicts our model, since the path from  $q$  to  $p$  is characterized by linear oscillators and by a time derivative: they are just linear filters and hence cannot explain the ‘rise’ of two spectral components in  $p$ .

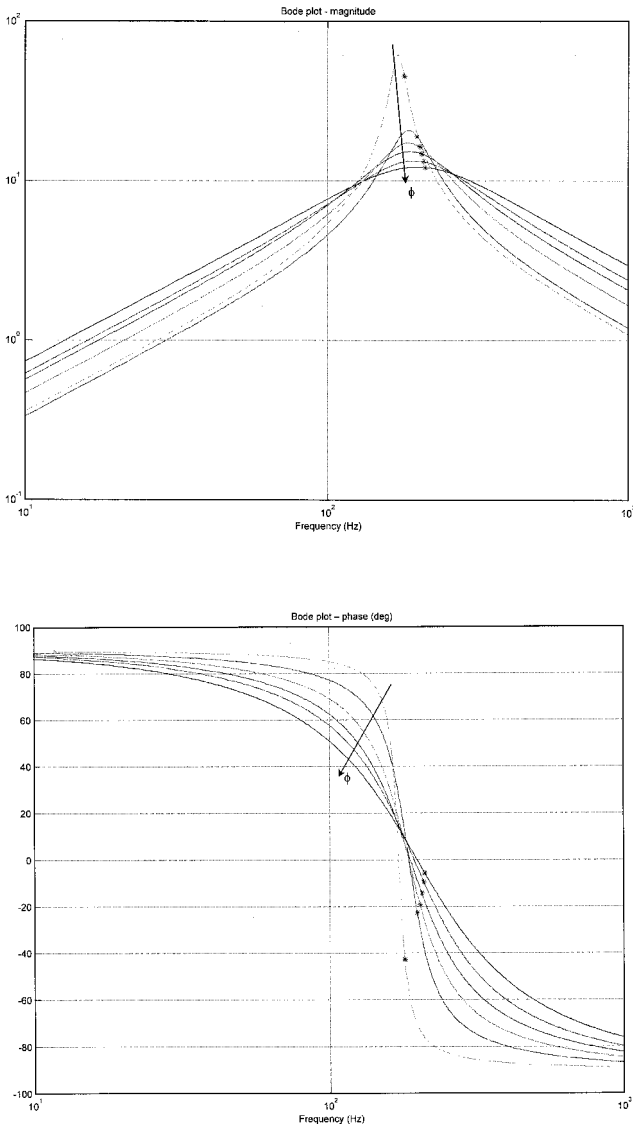


Figure 9. (a) Bode diagram (amplitude) of a non-falsified set of models  $G(s)$  (the measured points are indicated with '\*'). (b) Bode diagram (phase) of a set of non-falsified models  $G(s)$  (the measured points are indicated with '\*').

- The second main component of  $p$ , in terms of spectral energy, is a sinusoidal signal that is not harmonically related with the fundamental oscillation.

The seeming contradiction between the spectral content of  $q$  and  $p$  is explained by the fact that the measured signal  $q$  is not the 'true' heat release ratio but it is a low-pass filtered version of the actual  $q$ . The optical sensor used to infer heat release has a low-pass behaviour. Its cut-off frequency is just beyond 200 Hz. Note that a main consequence of the 'asymmetric' spectral content of  $p$  and  $q$  is the fact that a standard optimization-based identification of a parametric model (e.g. using maxi-

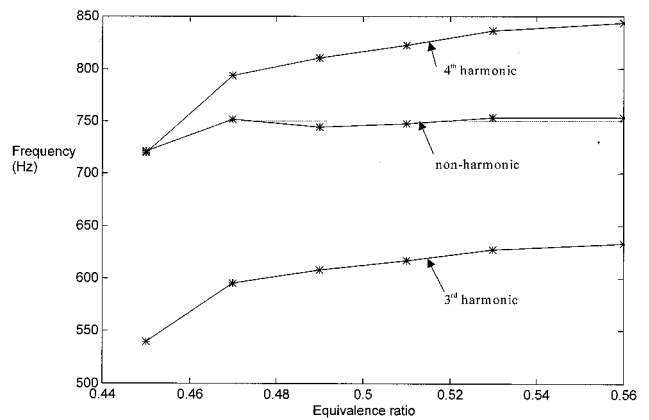


Figure 10. Frequency of the third harmonic, fourth harmonic and non-harmonic signals.

imum likelihood—see Ljung (1987)) based on I/O data is infeasible. An attempt in this direction was made in Murray *et al.* (1998), but the results were not satisfactory.

The second issue (the presence of a non-harmonic oscillation) is more subtle. To understand this problem better, the central frequency of this non-harmonic oscillation has been estimated in all the six experiments. The results are displayed in figure 10, where the frequency of the non-harmonic oscillation is compared with the frequency of the third and fourth harmonic signals. These results show a somewhat unexpected fact: in spite of comparatively large variations of the third and fourth harmonic frequencies, the frequency of the non-harmonic signal is almost invariant with  $\phi$ . Two questions must therefore be addressed:

- How can the presence of a large non-harmonic signal at that frequency be explained?
- Why the frequency of such a signal does not vary much with  $\phi$ ?

We propose a non-trivial but simple answer for both issues. They can be summarized as follows:

- The apparent non-harmonic oscillation corresponds to the frequency at which the Nyquist diagram of the linear part of the system crosses the negative real axis for a second time with magnitude greater than one. Since a system cannot support two non-harmonic limit cycles simultaneously, it is more likely that this represents the presence of two oscillatory attractors in the state with noise driving the exchange of energy between the two. This is also supported by the broader peak of the higher frequency signal. This is discussed in greater detail in Dunstan *et al.* (2000).

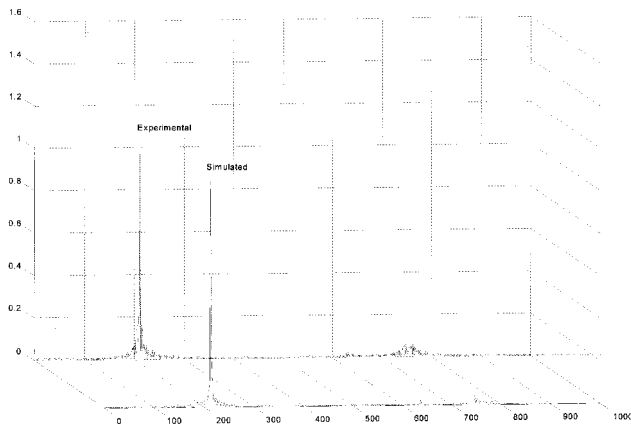


Figure 11. Measured (Experiment 1) and simulated power spectra of  $p$ .

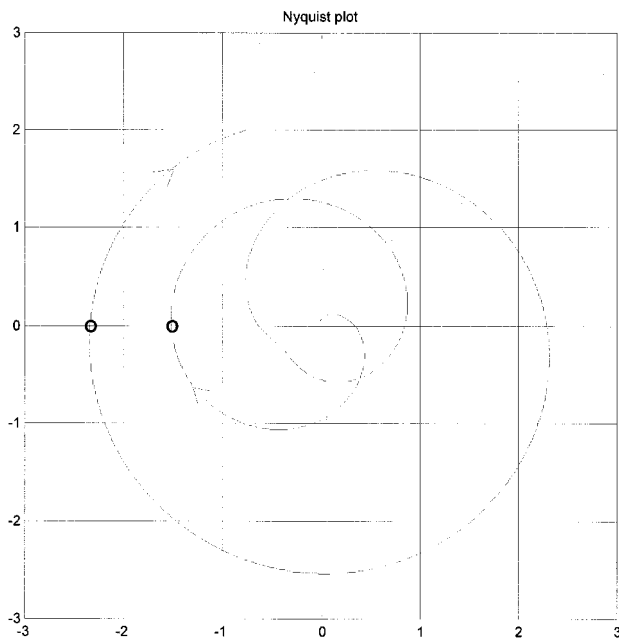


Figure 12. Nyquist plot of the linear part of the system. The two bullets are at 215 Hz (the inner one) and at 746 Hz (the outer one).

- Such a frequency is almost constant with respect to  $\phi$  since it mainly depends on the time delay  $\tau$  of the system. A  $\phi$ -independent  $\tau$  (see §3.1) hence yields a  $\phi$ -independent non-harmonic frequency.

In figure 11, the power spectrum of  $p$  produced by simulation with the two-oscillators system is displayed (using  $\tau = 0.00346$ ,  $\omega = 2\pi \cdot 215$ , and  $\xi = 0.2$ ). It is characterized by two sinusoidal signals: the first at 215 Hz, and the second at 746 Hz. Note that it reproduces almost perfectly the measured signal  $p$ . The possible occurrence of a second limit cycle is confirmed by

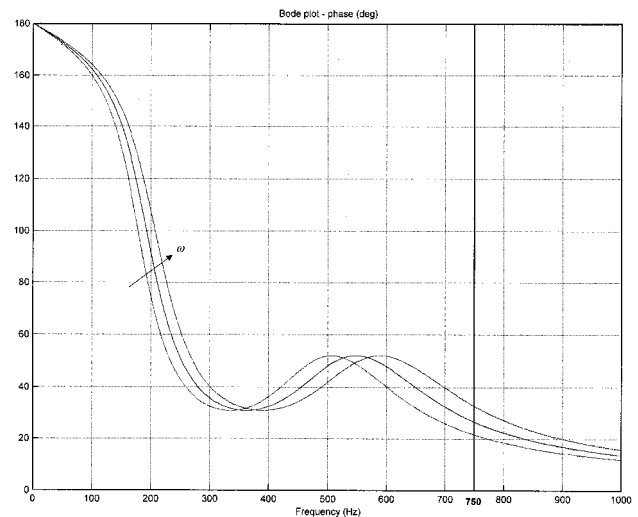
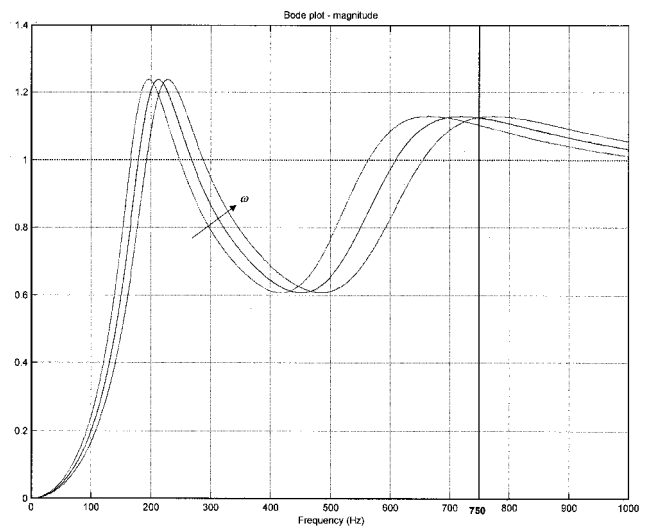


Figure 13. (a) Bode plot (magnitude) of the second-order oscillators, complemented with the double derivative part ( $\omega = 2\pi \cdot \{185, 200, 215\}$ ,  $\xi = 0.25$ ). (b) Bode plot (phase) of the second-order oscillators, complemented with the double derivative part ( $\omega = 2\pi \cdot \{185, 200, 215\}$ ,  $\xi = 0.25$ ).

the Nyquist plot of the linear part of the model (figure 12).

In order to gain some additional insight in this process, in figure 13 and 14 the Bode plots of the two linear parts of the model (the two oscillators complemented with the double derivative part—figure 13—and the time delay—figure 14) are displayed. Specifically, the second order oscillators are analysed for three different values of the central frequency ( $\omega = 2\pi \cdot \{185, 200, 125\}$ ,  $\xi = 0.25$ ), and the time delay is analysed for three slightly different values of  $\tau$  ( $\tau = \{0.00337, 0.00347, 0.00357\}$ ;  $\tau = 0.00347$  is the time delay actually estimated—see §3.1).

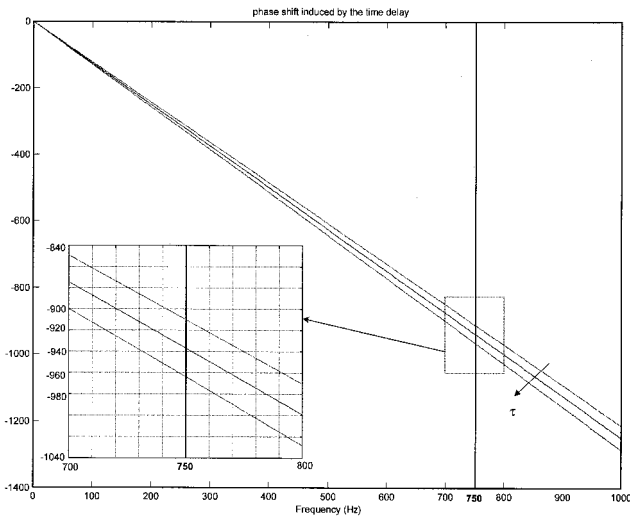


Figure 14. Bode plot (phase) of the time delay ( $\tau = \{0.003\ 37, 0.003\ 47, 0.003\ 57\}$ ).

The analysis of these Bode plots shows that:

- The presence of the two time-derivatives gives a very peculiar shape to the magnitude Bode plot of the linear part of the system: beyond the third acoustic resonance it is quite large and flat. This allows, at 750 Hz, a gain higher than 1 and a small sensitivity of the gain/phase of the loop transfer function with respect to variations of the fundamental frequency.
- The sum of the phase shift due to the linear parts of the model at 750 Hz is exactly  $-900^\circ$ : about  $+25^\circ$  due to the oscillators and the time derivatives (figure 13(b)) and  $-925^\circ$  due to the nominal time delay  $\tau = 0.003\ 47$  ms (figure 14). This phase shift is equivalent to  $-180^\circ$ : hence it is compatible with a permanent limit-cycling oscillation at 750 Hz.
- Because of the flatness of the magnitude of the Bode plot beyond the third acoustic mode, comparatively large variations in the central frequency of the acoustic modes (in figure 13 the effects of about 15% variations on  $\omega$  are shown) yield small variations in the phase shift at 750 Hz ( $10^\circ$ ). Instead, the effects of small changes in the time delay (in figure 14 the effects of about 3% variations on  $\tau$  are displayed) yield large phase variations (more than  $50^\circ$  at 750 Hz). This means that the spectral location of the non-harmonic signal is mainly determined by the time delay  $\tau$ . The fact that the time delay and the frequency of the harmonic signals are the only parameters of the model which appear to be independent of

$\phi$  is independent validation of the structure of the overall model.

## 5. Conclusions

In this paper the problem of fitting a set of data collected on a lean combustion process using a first-principles grey-box non-linear model has been considered. The main results obtained here are:

- Despite the paucity of information contained in the dominantly periodic data sets, the parameters of the model can be at least approximately estimated. The major indetermination, which cannot be resolved, is the phase and damping ratio of the second-order oscillators used to model the acoustic modes. Qualitative physical reasoning, however, reduces the set of unfalsified models.
- Even the high-frequency part of the measured signals can be explained and reproduced. Specifically, an explanation of the  $\phi$ -independent high-frequency non-harmonic oscillation has been proposed, which is consistent with the observed data sets, with the model structure, and with the dynamical properties between experiments.
- The data gathered are not informative enough to invalidate the proposed model. The ability of this simple model structure to support the data properties of limit cycling together with a non-harmonic spectral peak is surprising, all the more so because of the poor information content of the data from which the model was fitted. Nevertheless, one must remain sceptical of the identification process and look to develop feasible (in)validation tests. This subject is pursued in Dunstan *et al.* (2000). The data used here are simply insufficiently informative to invalidate the proposed model or its structure.

Finally, we wish to stress that the presence of multiple non-harmonically-related oscillatory attractors is the most surprising and interesting feature of the process we have considered. A preliminary analysis of this very unusual phenomenon, based on bifurcation theory, is proposed in Dunstan *et al.* (2000). The main outcome of such analysis is a set of guidelines for designing practically-feasible *ad hoc* experiments which can provide enough information to validate/invalidate/modify the model proposed herein. It is worth reiterating that, owing to the lack of information contained in the currently available data, one must be cautious how much is read into the results obtained without some further experimental validation.

## Acknowledgements

Research supported by USA National Science Foundation Grant ECS-0070146, and by CARIPLO Foundation for Scientific Research.

## References

- ANNASWAMY, A. M., and GHONIEM, A. F., 1995, Active control in combustion systems. *IEEE Control Systems Magazine*, 49–63.
- BALDINI, G., BITTANTI, S., DE MARCO, A., LONGHI, F., PONCIA, G., PRANDONI, W., and VETTORELLO, D., 1999, Modelling the nonlinear dynamics of combustion instabilities in gas turbines towards active control. *Proceedings of the 12th IFAC Triennial World Congress*, Beijing, China, Vol. O, pp. 79–84.
- BITMEAD, R., TSOI, A. C., and PARKER, P. J., 1986, A Kalman filtering approach to short-time Fourier analysis. *IEEE Transactions on Acoustic, Speech and Signal Processing*, **34**, 1493–1501.
- CULICK, F. E. C., 1976, Nonlinear behavior of acoustic waves in combustion chambers. *Acta Astronautica*, **3**, 715–757.
- DUNSTAN, W. J., BITMEAD, R. R., and SAVARESI, S. M., 2000, Validation test design for a nonlinear model developed from limit cycle data. *39th IEEE Conference on Decision and Control*, Sydney, Australia, pp. 1237–1242.
- GELB, A., and VAN DER VELDE, W. E., 1968, *Multiple-Input Describing Functions and Nonlinear System Design* (New York: McGraw-Hill).
- ISELLA, G., SEYWERT, C., CULICK, F. E. C., and ZUKOSKI, E. E., 1997, A further note on active control of combustion instabilities based on hysteresis. *Comb. Sci. Tech.*, **126**, 381–388.
- LJUNG, L., 1987, *System Identification* (Englewood Cliffs, NJ: Prentice-Hall).
- MURRAY, R. M., JACOBSON, C. A., CASAS, R., KHBIBNIK, A. I., JOHNSON JR., C. R., BITMEAD, R., PERACCHIO, A. A., and PROSCIA, W. M., 1998, System identification for limit cycling systems: a case study for combustion instabilities. *Proceedings of the American Control Conference*, Philadelphia, Pennsylvania, USA, pp. 2004–2008.
- PERACCHIO, A. A., and PROSCIA, W. M., 1998, Nonlinear heat-release/acoustic model for thermoacoustic instability in lean premixed combustors. Presented at *AMSE/IGTI Turbo Expo 1998*, Stockholm, Sweden.
- SAVARESI, S. M., BITMEAD, R. R., and DUNSTAN, W. J., 2000, Nonlinear system identification of a closed-loop lean combustion process. *12th IFAC Congress on System Identification*, Santa Barbara, CA, USA.
- YOUNG, P. C., 1999, Nonstationary time series analysis and forecasting. *Progress in Environmental Science*, **1**, 3–48.